J Mater Sci (2018) 53:2434–2442

Chemical routes to materials

Synthesis and characterization of ordered mesoporous silica using rosin-based Gemini surfactants

Wenkai Li[1], Danhua Xie[2], Binglei Song[1,*], Lin Feng[1], Xiaomei Pei[1], and Zhenggang Cui[1]

[1] Key Laboratory of Synthetic and Biological Colloids, Ministry of Education School of Chemical and Materials Engineering, Jiangnan University, Wuxi 214122, Jiangsu, People's Republic of China

[2] Fujian Province University Key Laboratory of Green Energy and Environment Catalysis, Fujian Provincial Key Laboratory of Featured Materials in Biochemical Industry, Ningde Normal University, Ningde 352100, Fujian, People's Republic of China

Received: 6 July 2017
Accepted: 11 October 2017
Published online: 23 October 2017

ABSTRACT

As structure-directing agents, the molecular structure of surfactants is critical for determining the properties of prepared mesoporous materials. Using dehydroabietic acid as a starting material, a series of rosin-based Gemini surfactants (abbreviated as R-*n*-R, $n = 3$, 6, 8 and 10, indicating the carbon atom number contained in the spacer) were synthesized and applied as templates in the preparation of ordered mesoporous silica. The structures and morphologies of the samples were characterized by X-ray diffraction, scanning electron microscope, transmission electron microscope and N_2 adsorption–desorption. The R-*n*-R surfactants feature rigid tricyclic hydrophobic groups with large volumes, which are beneficial for the formation of a three-dimensional cubic phase. Furthermore, the spacer length was found to have a tremendous effect on the structure of the prepared mesoporous silica materials. The head group of R-3-R, which has a short spacer, is excessively charged, leading to silica nanoparticles with an irregular morphology and a rather low BET surface area. With longer spacer lengths, R-6-R, R-8-R and R-10-R are conducive to generating silica nanoparticles with a novel dumbbell-like morphology and with higher BET surface areas of 1171, 1096 and 1186 $m^2 g^{-1}$, respectively. The results demonstrate the particularities of the Gemini surfactant structure in the preparation of mesoporous silica nanoparticles with novel morphologies, and the details of the molecular interactions that occur in the condensation of silicate anions are also revealed.

Address correspondence to E-mail: ccfsbl@jiangnan.edu.cn

DOI 10.1007/s10853-017-1709-y

Introduction

Ordered mesoporous materials feature novel morphologies, highly ordered nanostructures, and high specific areas and channel volumes [1–3]. They have been widely applied in catalysis [4–6], drug carriers [7–9], enzyme immobilization [10], optoelectronic devices [11] and the preparation of multifunctional microreactors [12]. The preparation of mesoporous materials generally follows a supramolecular template mechanism. The morphologies of the resulting mesoporous materials are thus affected by many factors such as the surfactant structure, reactant ratio, temperature and pH [13–15]. As structure-directing agents, surfactants are recognized to have a tremendous effect on the structures of prepared mesoporous materials. This issue has been addressed in many references [16–18] by investigating surfactants with different structures.

Gemini surfactants have received considerable attention in recent years [19–21]. They consist of two head groups, two hydrophobic chains and a spacer linked at or near the head groups [22]. Because of this unique molecular structure, Gemini surfactants are known to form novel aggregates in solution [23, 24]. Gemini surfactants are also utilized as templates in the preparation of mesoporous materials with specific properties [25, 26]. Li et al. [27] prepared hollow mesoporous silica particles with large pore volumes using Gemini surfactant $C_{14\text{-}2\text{-}14}$. This material is suitable for drug delivery and catalysis applications. In another study, Hao et al. [28] obtained *Fm*3*m*-type chiral mesoporous silica with face-centered symmetry using mixtures of P123 and quaternary ammonium Gemini surfactants with different spacer lengths as the templates. A pumpkin morphology was observed. Relying on a series of asymmetric Gemini surfactants $C_{n\text{-}s\text{-}m}$, three-dimensional hexagonal-arrayed mesostructure supercages were obtained by Huo et al. [16]. It is clear that using novel Gemini surfactants as templates is beneficial for obtaining mesoporous materials with new morphologies and properties.

Rosin is composed of resin acids with diterpenoid structures. Dehydroabietic acid is one of the important derivatives of rosin and features a rigid tricyclic skeleton [29, 30]. A Gemini surfactant molecule containing the dehydroabietic acid as the hydrophobic group is expected to have a large molecular packing parameter [31], leading to the aggregates with lower curvatures. Such aggregates are related with the morphology, the pore size and distribution of resulted mesoporous materials. However, since the mesoporous materials templated from rosin-based surfactants were rare up to now [32], the effect of this molecular feature on the synthesis of mesoporous materials has never been considered. In this work, a series of Gemini surfactants containing dehydroabietic acid units were synthesized using dehydroabietic acid as the starting material. Several ordered mesoporous silicas were prepared using these new Gemini surfactants as the templates. Different with the 2D hexagonal samples prepared with single-head rosin-based surfactant [32], the 3D cubic mesoporous silicas were obtained. The relationships between the structures of mesoporous materials and the surfactant structures were revealed.

Table 1 The *d* values of four mesoporous silica samples prepared using R-*n*-R as the template

d (nm)	211	220
R-3-R		
R-6-R	3.43	2.98
R-8-R	3.51	2.95
R-10-R	3.28	2.74

Experimental methods

Chemicals

Ethyl silicate (AR), anhydrous ether (AR), aqueous ammonia (AR), thionyl chloride (AR) and triethylamine (AR) were purchased from Sinopharm Chemical Reagent Co., Ltd. 3-(Dimethylamino)-1-propylamine (99.0%) was obtained from Aladdin Chemistry Co., Ltd. α,ω-Dibromoalkanes (97.0%) were purchased from Tokyo Chemical Industry Co., Ltd. Disproportionated rosin was purchased from Nanjing Pine Forests Chemistry Co., Ltd. Dehydroabietic acid (97.9%) was obtained by purifying the disproportionated rosin in our laboratory.

Synthesis of Gemini surfactants R-*n*-R

The detailed synthetic procedures for Gemini surfactants (abbreviated as R-*n*-R, $n = 3$, 6, 8 and 10, indicating the carbon atom number contained in the spacer) are described in Fig. 1. A brief description of

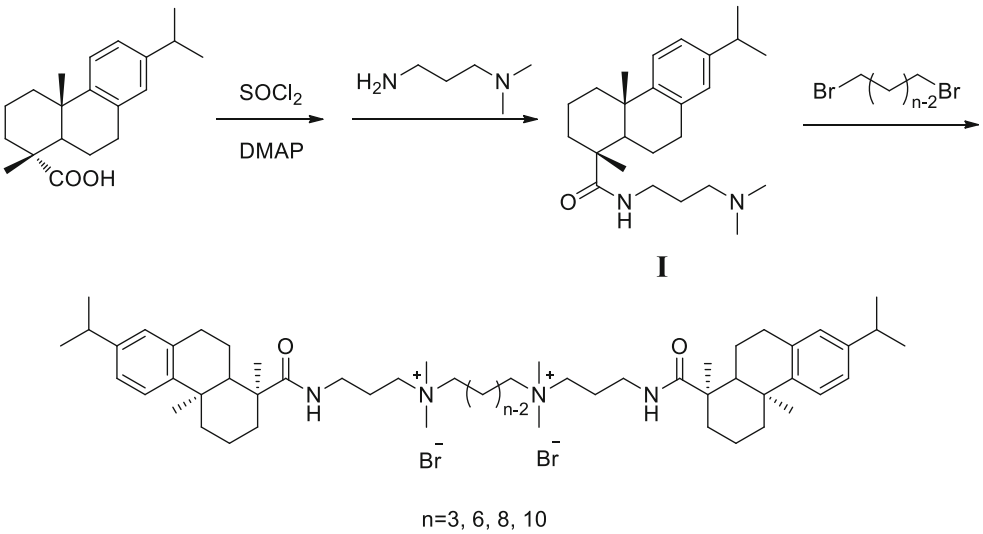

Figure 1 Synthetic route to rosin-based Gemini surfactants R-*n*-R.

the synthetic procedure is as follows: Dehydroabietic acid was first transformed to its corresponding chloride by reaction with $SOCl_2$ in the presence of 4-dimethylaminopyridine (DMAP). The chloride was reacted with 3-(dimethylamino)-1-propylamine in an ice bath for 2 h in the presence of trimethylamine to give 3-(N,N-dimethyl)-propyl dehydroabietamide (**I**). This intermediate **I** was first purified by column chromatography and then reacted with α,ω-dibromoalkanes at 80 °C in ethanol solution for 36 h. After the reaction was completed, the solvent was removed under reduced pressure. The residue was recrystallized three times from a mixture of ethanol and ethyl acetate. The final product was obtained as white solid after drying under vacuum at 55 °C. The ^{1}H NMR analyses of the compounds are as follows:

R-3-R: ^{1}H NMR (400 MHz, DMSO) δ 7.77 (t, 2H), 7.16 (d, 2H), 7.01–6.94 (m, 2H), 6.83 (d, 2H), 3.30–3.23 (m, 8H), 3.20–3.09 (m, 4H), 3.06 (s, 12H), 2.85–2.70 (m, 6H), 2.29 (d, 2H), 2.15 (m, 2H), 2.06–1.99 (m, 2H), 1.91–1.80 (m, 4H), 1.76–1.58 (m, 8H), 1.47 (d, 2H), 1.40–1.29 (m, 4H), 1.18 (s, 6H), 1.16 (s, 6H), 1.14 (d, 12H).

R-6-R: ^{1}H NMR (400 MHz, DMSO) δ 7.76 (t, 2H), 7.17 (d, 2H), 7.01–6.95 (m, 2H), 6.84 (d, 2H), 3.28–3.18 (m, 8H), 3.17–3.09 (m, 4H), 3.01 (s, 12H), 2.85–2.70 (m, 6H), 2.30 (d, 2H), 2.06–2.00 (m, 2H), 1.86–1.77 (m, 4H), 1.76–1.59 (m, 12H), 1.46 (d, 2H), 1.41–1.27 (m, 8H), 1.18 (s, 6H), 1.17 (s, 6H), 1.15 (d, 12H).

R-8-R: ^{1}H NMR (400 MHz, DMSO) δ 7.74 (t, 2H), 7.17 (d, 2H), 7.01–6.95 (m, 2H), 6.83 (d, 2H), 3.26–3.16 (m, 8H), 3.16–3.09 (m, 4H), 2.99 (s, 12H), 2.85–2.70 (m, 6H), 2.29 (d, 2H), 2.05–1.99 (m, 2H), 1.85–1.76 (m, 4H), 1.75–1.56 (m, 12H), 1.45 (d, 2H), 1.41–1.22 (m, 12H), 1.17 (s, 6H), 1.16 (s, 6H), 1.14 (d, 12H).

R-10-R: ^{1}H NMR (400 MHz, DMSO) δ 7.75 (t, 2H), 7.16 (d, 2H), 7.01–6.95 (m, 2H), 6.83 (d, 2H), 3.28–3.17 (m, 8H), 3.16–3.10 (m, 4H), 3.00 (s, 12H), 2.85–2.70 (m, 6H), 2.29 (d, 2H), 2.06–2.00 (m, 2H), 1.85–1.77 (m, 4H), 1.75–1.55 (m, 12H), 1.46 (d, 2H), 1.38–1.22 (m, 16H), 1.17 (s, 6H), 1.16 (s, 6H), 1.14 (d, 12H).

Materials

In a typical preparation of mesoporous silica, a certain amount of rosin-based Gemini surfactant was first dissolved in deionized water at 303 K. Anhydrous ether was added under vigorous stirring. The volume ratio of deionized water to anhydrous ether was 1.2:1. The pH of the mixed solution was adjusted using aqueous ammonia. Ethyl silicate was then added under stirring at 303 K. The molar composition of the mixture was TEOS/surfactant/H_2O = 1:0.075–0.25:250. After reacting for 24 h, the reaction mixture was transferred to a Teflon-lined autoclave and incubated at 373 K for 36 h. The result solid was washed with water and ethanol several times and dried at 363 K. The final product was obtained by calcination at 823 K for 5 h with a rate of 2 K min^{-1}.

Characterization

Powder small-angle X-ray diffraction (XRD) data were acquired on a Bruker AXS D8 diffractometer with a Cu target at 40 kV and 40 mA using a

scanning speed of 2° min^{-1} and a step of 0.02°. Transmission electron microscope (TEM) images were obtained using a JEOL JEM-2100 electron microscope operating at 300 kV. Scanning electron microscope (SEM) images were recorded with a Hitachi S-4800 instrument operated at 2.0 kV. Nitrogen adsorption–desorption isotherms of the samples were determined at 77 K using a Micromeritics ASAP 2020 MP instrument. Surface areas were calculated using the BET method. The pore distributions were plotted using the BJH method, and the total pore volume was calculated from the amount adsorbed at a relative pressure (P/P_0) of approximately 0.99.

Results and discussion

To explore the appropriate conditions for preparing mesoporous materials, the surfactant R-6-R was first investigated. The small-angle XRD patterns of the calcined products prepared with different R-6-R/TEOS mole ratios are shown in Fig. 2. When the R-6-R/TEOS ratio was 0.075:1, the sample presented only one strong diffraction peak in the small-angle region (Fig. 2a), indicating the formation of a short-range-ordered pore structure. By increasing the molar ratio of R-6-R, the regularity of the pore structure was enhanced. When the R-6-R/TEOS mole ratio reached 0.1:1, two strong peaks (Fig. 2b) emerged at $2\theta = 2.57°$ and 2.96° with corresponding d values of 3.43 and 2.98 nm. The other diffuse patterns observed at $2\theta = 4.06°$, 4.32°, 4.81°, 5.18° and 5.44° with corresponding d values of 2.17, 2.04, 1.84, 1.70 and 1.62 nm were indexed as (321), (400), (420), (332) and (422) reflections, indicating the presence of the cubic phase silica (PDF card no: 50-0511). The ratio between reciprocal d-spacing of the peaks assigned as (211) and (220) is 0.87, which is consistent with the 3D cubic lattice symmetry (space group $Ia3d$ symmetry). The unit-cell parameter a_0 of the cubic system was calculated by formula $a = d\,(h^2 + k^2 + l^2)^{1/2}$, and the a_0 value was 8.40 nm. However, further increasing the molar ratio of R-6-R led to a reduction in the regularity of the pore structures. Therefore, the molar ratio of the surfactant and TEOS was fixed at 0.1:1 when investigating other products from R-n-R with different spacer lengths.

The small-angle XRD patterns of the calcined products prepared using R-6-R as the template at different original pH values are displayed in Fig. 3. The pH values of the present systems were adjusted with aqueous ammonia. At pH = 11.0, the obtained product exhibited only one strong peak at $2\theta = 2.28°$ (Fig. 3c) in the XRD pattern. When the original pH value was decreased to 10.5, the sample presented two strong peaks as illustrated in Fig. 3b, which

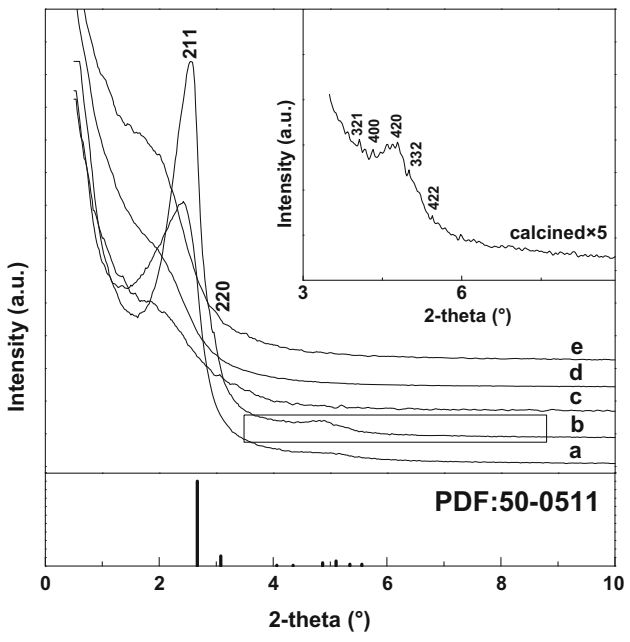

Figure 2 Small-angle XRD patterns of calcined mesoporous silicas prepared with different R-6-R/TEOS mole ratios: *a* 0.075:1, *b* 0.10:1, *c* 0.15:1, *d* 0.20:1 and *e* 0.25:1. The samples were all synthesized at the same original pH value (10.5). Inset: Low-intensity XRD peaks of sample **b**.

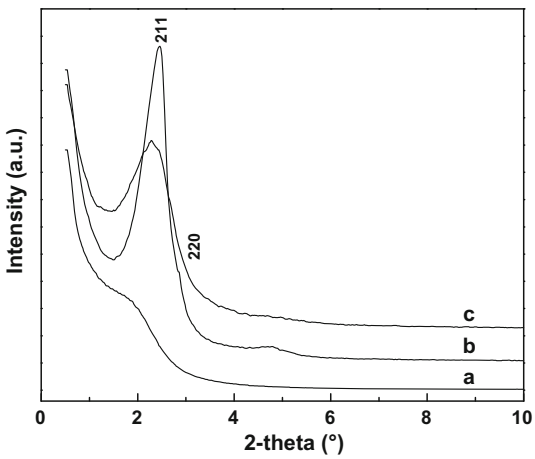

Figure 3 Small-angle XRD patterns of the calcined mesoporous silicas prepared at different pH values: *a* 10.0, *b* 10.5 and *c* 11.0. The samples were synthesized using the same R-6-R/TEOS mole ratio (0.10:1).

indicates an improvement in the regularity of the mesostructure. The sample exhibited only one broad peak at pH = 10.0, revealing a decrease in the regularity. When the pH value was lower than 9.0 or higher than 12.0, almost no product was obtained. This means that for the present systems, the original pH value of 10.5 is suitable for preparing mesoporous materials with regular pore structures.

Silica nanoparticles were then synthesized using rosin-based Gemini surfactants with different spacer lengths at the same mole ratio R-*n*-R/TEOS = 0.10:1 and at a pH of 10.5. The morphology of the particles was observed using a scanning electron microscopy (SEM). The results are depicted in Fig. 4. Nanoparticles with irregular morphologies were observed for the R-3-R-templated samples (Fig. 4a). With longer spacer lengths, regular nanoparticles of approximately 150–200 nm with dumbbell-like morphologies dominated the entire visual field (Fig. 4b–d). Several spherical particles were also observed. The formation of a dumbbell-like morphology is obviously attributed to the fusion of initially generated spherical nanoparticles. In a previous study, Lebedev et al. [33, 34] observed that under hydrothermal treatment, the surface of an incompact silica network partially dissolves, leading to structure reconstruction. Two adjacent particles are thus connected by the dissolved silica to form a dumbbell-like morphology with a more condensed silica network. To the best of our knowledge, such a morphology is rare among the reported mesoporous silica nanoparticles. Furthermore, several hollow nanoparticles were identified in the TEM images (Fig. 6b) of the samples prepared using R-6-R as the template. This is attributed to Ostwald ripening [35, 36] after the formation of the nanoparticles.

Figure 5 presents the small-angle XRD patterns of four calcined mesoporous silica samples synthesized at the same mole ratio and pH. Their d values are shown in Table 1. For the mesoporous silica sample templated using the Gemini surfactant R-3-R, only a shoulder-like peak at $2\theta = 1.87°$ appeared, indicating poor regularity of the mesostructure. Upon increasing the number of carbon atoms in the spacer to 6, a strong peak at 2.57°, together with a weak peak at 2.96°, appeared, indicating that the regularity of the pore structure was enhanced significantly. Upon further increasing the length of the spacer group, the resulting silica nanoparticles exhibited two small peaks at 3.01° and 3.21° in addition to the major

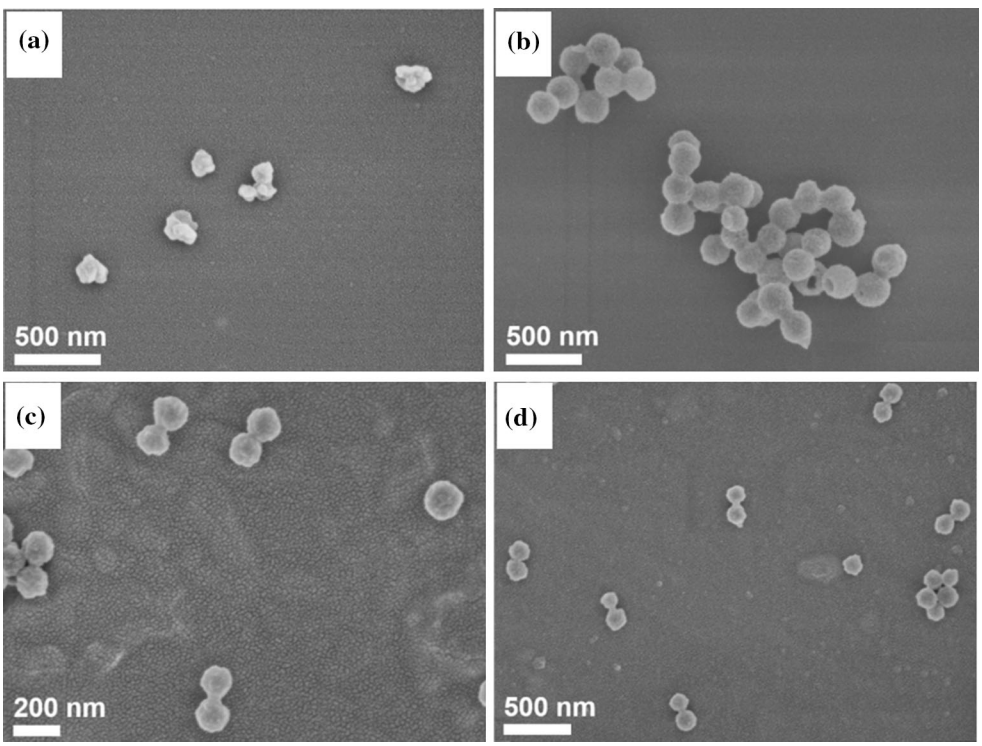

Figure 4 SEM images of the calcined mesoporous silicas prepared using rosin-based Gemini surfactants **a** R-3-R, **b** R-6-R, **c** R-8-R and **d** R-10-R. The samples were synthesized using the same mole ratio R-*n*-R/TEOS = 0.10:1 and at a pH of 10.5.

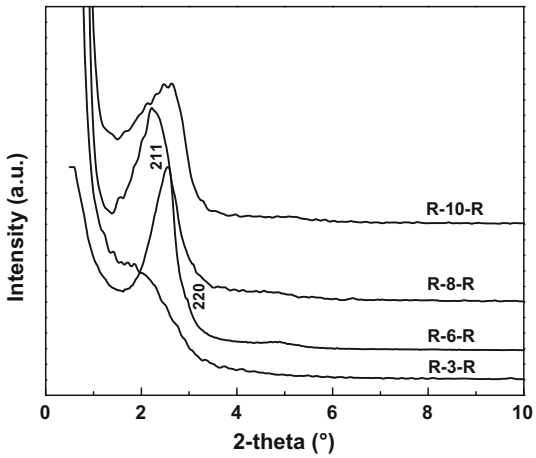

Figure 5 Small-angle XRD patterns of the calcined mesoporous silicas prepared using rosin-based Gemini surfactants *a* R-3-R, *b* R-6-R, *c* R-8-R and *d* R-10-R.

peaks. The XRD patterns displayed in Fig. 5 indicate that the R-6-R-, R-8-R- and R-10-R-templated mesoporous nanoparticles all possess a 3D cubic phase. It was reported that Gemini surfactants with a spacer length of 10–12 carbon atoms can yield the cubic MCM-48 phase and that smaller spacers prefer the hexagonal MCM-41 phase [37, 38]. Nevertheless, the spacer of R-6-R, which contains only six carbon atoms, tends to form the 3D cubic phase. The formation of the 3D cubic phase can be related to the molecular effective packing parameter $P = V/a_0 l$ [14], where V is the total volume of hydrophobic chains, a_0 is the effective head group area at the micelle surface, and l is the length of the extended alkyl tail chain. The 3D cubic phase is preferred if the molecular effective packing parameter of the template is large enough. The extremely long spacers of a Gemini surfactant tend to bend toward the hydrophobic core in an aggregate. The hydrophobic group volume is thus increased, leading to a larger packing parameter. However, for the present investigated systems, mesoporous nanoparticles with a 3D cubic phase have been discovered even though the spacer of the template molecule contains only six carbon atoms. Obviously, the reason is attributed to the unique molecular structure of R-*n*-R. The hydrophobic group of R-*n*-R features a large phenanthrene skeleton, which is responsible for a large value of V. Compared to Gemini surfactants with flexible hydrophobic chains [14, 38, 39], the molecular effective packing parameter of R-*n*-R is already large enough regardless of the spacer length. The formation of a 3D cubic phase in the nanoparticles is thus preferred.

The formation of a highly ordered mesostructure was further confirmed by TEM analysis. Figure 6 displays the transmission electron microscopy (TEM) images of the calcined mesoporous silica samples prepared using four rosin-based Gemini surfactants with different spacer lengths. The poor regularity of the mesoporous silica sample prepared using R-3-R

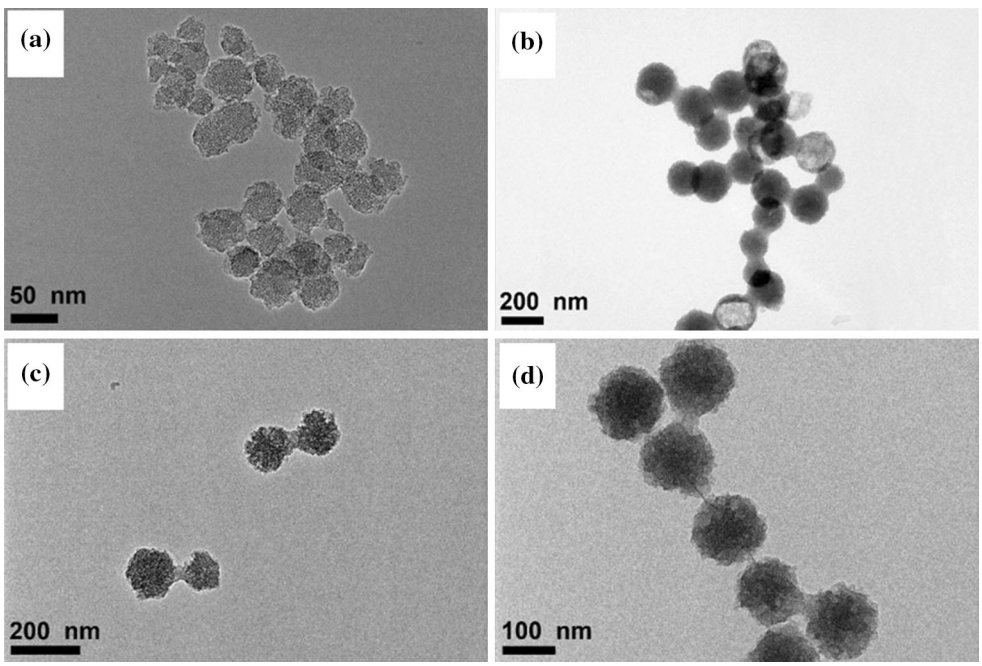

Figure 6 TEM images of the calcined mesoporous silicas prepared using rosin-based Gemini surfactants **a** R-3-R, **b** R-6-R, **c** R-8-R and **d** R-10-R.

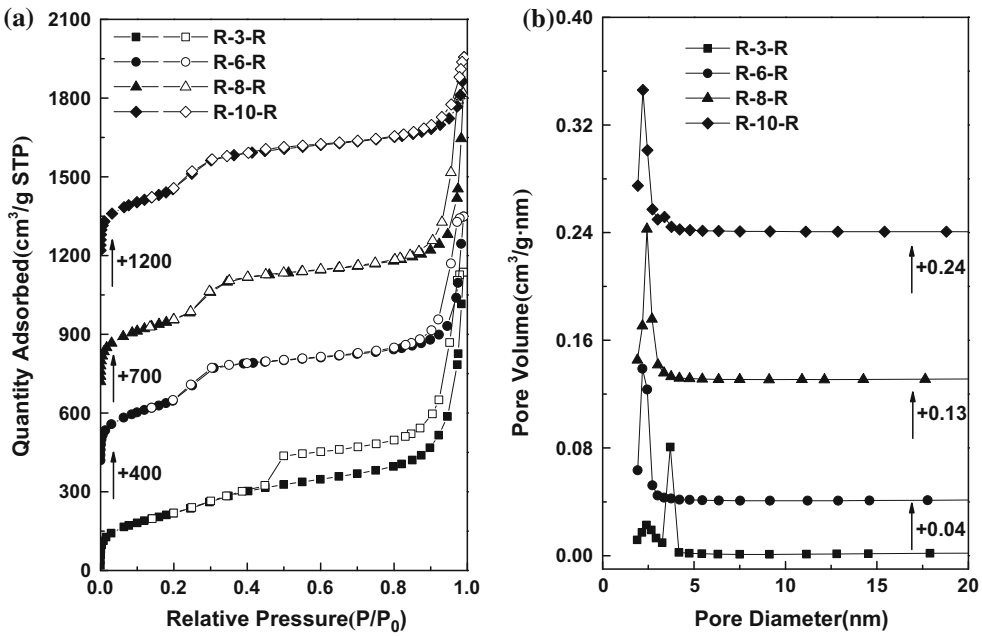

Figure 7 **a** N_2 adsorption–desorption isotherms (Filled symbols represent adsorption isotherms and open symbols represent desorption isotherms) and **b** BJH pore size distributions of the calcined mesoporous silicas prepared using rosin-based Gemini surfactants R-3-R, R-6-R, R-8-R and R-10-R.

Table 2 Characteristics of four mesoporous silica samples prepared using R-*n*-R as the template

R-*n*-R	S_{BET} (m^2 g^{-1})	V (cm^3 g^{-1})	D_p (nm)
R-3-R	822	1.75	3.70
R-6-R	1171	1.47	2.28
R-8-R	1096	1.73	2.43
R-10-R	1186	1.15	2.22

as the template can be clearly observed. In contrast, the other three samples exhibit a regular and ordered structure of the mesoporous channels.

Figure 7a presents the nitrogen adsorption–desorption isotherms of the calcined mesoporous silica samples. The isotherms are of type IV according to the IUPAC classification, and the curves show hysteresis loops due to capillary condensation at a relative pressure, P/P_0, of 0.30. The curves are linear within the P/P_0 range of 0.05–0.25. When P/P_0 is higher than 0.25, the curves deviate significantly from linearity. Therefore, the P/P_0 range 0.05–0.25 was selected for calculating the BET surface areas. The narrow pore diameter distributions of the calcined silica samples that were calculated using the Barrett–Joyner–Halenda (BJH) model are illustrated in Fig. 7b. The corresponding data are listed in Table 2. As revealed by the SEM, XRD and TEM results, the R-3-R-templated sample shows the most irregular morphology and the least ordered mesostructure. The BET surface area of this sample is 822 m^2 g^{-1}, which is also the smallest among the investigated mesoporous nanoparticles. The other three samples exhibited BET surface areas of approximately 1100 m^2 g^{-1}, which is comparable to products templated using conventional surfactants with flexible hydrophobic chains [28, 39, 40]. It is also clear from Table 2 that a small BET surface area corresponds to a large pore size.

The above experimental results reveal that the Gemini surfactant R-3-R with a short spacer is unable to generate nanoparticles with a regular morphology. Compared to the other homologues, this surfactant is also unfavorable for the generation of well-ordered mesoporous nanoparticles with large BET surface areas. This indicates that the spacer length in a Gemini surfactant has a tremendous effect on the properties of the resulting mesoporous nanoparticles. Zana et al. [41] investigated the effect of spacer length on the aggregation of Gemini surfactants in detail. The thermodynamic distance of the ionic surfactants packed at the surface of the aggregates is approximately 0.7–0.9 nm, which is equal to the length of a polymethylene spacer containing 6–7 carbon atoms. If the spacer length between the two head groups in a Gemini surfactant is shorter than this distance, the charge density of the head groups would be greatly enhanced. The spacer of R-3-R, which contains only three carbon atoms, is considered to hold the head groups tightly, resulting in a high charge density. The formation of mesoporous materials is a synergistic

assembly process of surfactants and silicate anions. The positively charged head group of R-3-R with a high charge density induces faster aggregation and condensation of silicate anions at the composite aggregate surface before they can arrange in order. The resulting morphology of the mesoporous material thus becomes irregular. The mesoporous pores are also less ordered with a random pore size distribution. The adsorption ability is also decreased.

Conclusions

Ordered cubic mesoporous silicas have been successfully synthesized using a series of newly synthesized rosin-based Gemini surfactants as templates and TEOS as a silicon source. Unlike conventional surfactants, rosin-based Gemini surfactants possess a rigid tricyclic structure that has a large volume and behaves as a hydrophobic group, which is beneficial for the formation of a three-dimensional cubic phase. The regularity of the pore structure relies heavily on the mole ratio of the template to the silicon source as well as on the pH of the system. The spacer length of the Gemini surfactant was found to have a tremendous effect on the morphology of prepared mesoporous materials. The synthesized materials are expected to have applications in separations, catalysis and drug delivery on account of their novel morphology and size selectivity.

Acknowledgements

Support from the National Natural Science Foundation of China (31300486) and the open research fund of Jiangsu Province Biomass Energy and Materials Laboratory (JSBEM201501) is gratefully acknowledged.

Compliance with ethical standards

Conflict of interest The authors declare that they have no conflict of interest.

References

[1] Kresge C, Leonowicz M, Roth W, Vartuli J, Beck J (1992) Ordered mesoporous molecular sieves synthesized by a liquid-crystal template mechanism. Nature 359(6397):710–712

[2] Beck J, Vartuli J, Roth W, Leonowicz M, Kresge C, Schmitt K, Mccullen S (1992) A new family of mesoporous molecular sieves prepared with liquid crystal templates. J Am Chem Soc 114(27):10834–10843

[3] Wu S, Mou C, Lin H (2013) Synthesis of mesoporous silica nanoparticles. Chem Soc Rev 42(9):3862–3875

[4] Corma A (1997) From microporous to mesoporous molecular sieve materials and their use in catalysis. Chem Rev 97(6):2373–2420

[5] Pastva J, Skowerski K, Czarnocki S, Žilková N, Čejka J, Bastl Z, Balcar H (2014) Ru-based complexes with quaternary ammonium tags immobilized on mesoporous silica as olefin metathesis catalysts. ACS Catal 4(4):3227–3236

[6] Ji B, Dahl M, Li N, Zaera F, Yin Y (2013) Tailored synthesis of mesoporous TiO_2 hollow nanostructures for catalytic applications. Energy Environ Sci 6(7):2082–2092

[7] Angelova A, Angelov B, Mutafchieva R, Lesieur S (2015) Biocompatible mesoporous and soft nanoarchitectures. J Inorg Organomet Polym 25(2):214–232

[8] Angelova A, Angelov B, Drechsler M, Lesieur S (2013) Neurotrophin delivery using nanotechnology. Drug Discov Today 18(23–24):1263–1271

[9] Zerkoune L, Lesieur S, Putaux J, Choisnard L, Angelov B, Doutch J, Angelova A (2016) Mesoporous self-assembled nanoparticles of biotransesterified cyclodextrins and non-lamellar lipids as carriers of water-insoluble substances. Soft Matter 12(36):7539–7550

[10] Kalantari M, Yu M, Yang Y, Strounina E, Gu Z, Yu C (2016) Tailoring mesoporous-silica nanoparticles for robust immobilization of lipase and biocatalysis. Nano Res 10(2):605–617

[11] Crossland E, Noel N, Sivaram V, Leijtens T, Alexander-Webber J, Snaith H (2013) Mesoporous TiO_2 single crystals delivering enhanced mobility and optoelectronic device performance. Nature 495(7440):215–219

[12] Zhang L, Xing Z, Zhang H, Li Z, Wu X, Zhang X, Zhang Y, Zhou W (2016) High thermostable ordered mesoporous SiO_2–TiO_2 coated circulating-bed biofilm reactor for unpredictable photocatalytic and biocatalytic performance. Appl Catal B-Environ 180:521–529

[13] Hunks W, Ozin G (2005) Challenges and advances in the chemistry of periodic mesoporous organosilicas (PMOs). J Mater Chem 15(35):3716–3724

[14] Huo Q, Margolese D, Stucky G (1996) Surfactant control of phases in the synthesis of mesoporous silica-based materials. Chem Mater 8(5):1147–1160

[15] Miyasaka K, Han L, Che S, Terasaki O (2006) A lesson from the unusual morphology of silica mesoporous crystals: growth and close packing of spherical micelles with multiple twinning. Angew Chem Int Ed 118(39):6666–6669

[16] Huo Q, Leon R, Petroff P, Stucky G (1995) Mesostructure design with Gemini surfactants: supercage formation in a three-dimensional hexagonal array. Science 268(5215):1324–1327

[17] Zhao D, Huo Q, Feng J, Jiman K, Han Y, Stucky G (1999) Novel mesoporous silicates with two-dimensional mesostructure direction using rigid bolaform surfactants. Chem Mater 11(10):2668–2672

[18] Tanev P, Pinnavaia T (1995) A neutral templating route to mesoporous molecular sieves. Science 267(5199):865–867

[19] Liao X, Gao Z, Xia Y, Niu F, Zhai W (2017) Rational design and synthesis of carboxylate Gemini surfactants with excellent aggregate behaviour for nano-La_2O_3 morphology-controllable preparation. Langmuir 33(13):3304–3310

[20] Lei L, Feng L, Song B, Zhai Z, Shang S, Song Z (2016) Ionic liquid crystals with novel thermal properties formed by the Gemini surfactants containing four hydroxyl groups. RSC Adv 6(101):99361–99366

[21] Bhadani A, Tani M, Endo T, Sakai K, Abe M, Sakai H (2015) New ester based Gemini surfactants: the effect of different cationic headgroups on micellization properties and viscosity of aqueous micellar solution. Phys Chem Chem Phys 17(29):19474–19483

[22] Menger F, Littau C (1991) Gemini surfactants: synthesis and properties. J Am Chem Soc 113(4):1451–1452

[23] Menger F, Keiper J (2000) Gemini surfactants. Angew Chem Int Ed 39(11):1906–1920

[24] Zana R, Xia J (2004) Gemini surfactants: synthesis, interfacial and solution-phase behavior, and applications. Marcel Dekker Inc, New York

[25] Shen S, Garcia-Bennett A, Liu Z, Lu Q, Shi Y, Yan Y, Terasaki O (2005) Three-dimensional low symmetry mesoporous silica structures templated from tetra-headgroup rigid bolaform quaternary ammonium surfactant. J Am Chem Soc 127(18):6780–6787

[26] Ryoo R, Park I, Jun S, Lee C, Kruk M, Jaroniec M (2005) Synthesis of ordered and disordered silicas with uniform pores on the border between micropore and mesopore regions using short double-chain surfactants. J Am Chem Soc 123(8):1650–1657

[27] Li M, Zhang C, Yang X, Xu H (2013) Controllable synthesis of hollow mesoporous silica nanoparticles templated by kinetic self-assembly using a Gemini surfactant. RSC Adv 3(37):16304–16307

[28] Hao T, Shi J, Zhuang T, Wang W, Li F, Wang W (2012) Mesostructure-controlled synthesis of chiral norbornane-bridged periodic mesoporous organosilicas. RSC Adv 2(5):2010–2014

[29] Wang H, Nguyen T, Li S, Liang T, Zhang Y, Li J (2015) Quantitative structure-activity relationship of antifungal activity of rosin derivatives. Bioorg Med Chem Lett 25(2):347–354

[30] González M, Pérezguaita D, Correarroyero J, Zapata B, Agudelo L, Mesaarango A, Betancurgalvis L (2010) Synthesis and biological evaluation of dehydroabietic acid derivatives. Eur J Med Chem 45(2):811–816

[31] Israelachvili J, Mitchell D, Ninham B (1976) Theory of self-assembly of hydrocarbon amphiphiles into micelles and bilayers. J Chem Soc Faraday Trans II 72(24):1525–1568

[32] Wang P, Chen S, Zhao Z, Wang Z, Fan G (2015) Synthesis of ordered porous SiO_2 with pores on the border between the micropore and mesopore regions using rosin-based quaternary ammonium salt. RSC Adv 5(15):11223–11228

[33] Lebedev O, Turner S, Liu S, Cool P, Van T (2012) New nano-architectures of mesoporous silica spheres analyzed by advanced electron microscopy. Nanoscale 4(5):1722–1727

[34] Liu S, Lebedev O, Mertens M, Meynen V, Cool P, Tendeloo G, Vansant E (2008) The merging of silica-surfactant microspheres under hydrothermal conditions. Microporous Mesoporous Mat 116(1):141–146

[35] Lou X, Wang Y, Yuan C, Lee J, Archer L (2006) Template-free synthesis of SnO_2 hollow nanostructures with high lithium storage capacity. Adv Mater 18(17):2325–2329

[36] Liu B, Zeng H (2005) Symmetric and asymmetric Ostwald ripening in the fabrication of homogeneous core-shell semiconductors. Small 1(5):566–571

[37] Voort P, Mathieu M, Mees F, Vansant E (1998) Synthesis of high-quality MCM-48 and MCM-41 by means of the Gemini surfactant method. J Phys Chem B 102(44):8847–8851

[38] Han S, Hou W, Xu J, Huang X, Zheng L (2006) Study of the *Pm*3*n* space group of cubic mesoporous silica. Chem Phys Chem 7(2):394–399

[39] Lee H, Pak C, Yi S, Shon J, Kim S, So B, Chang H, Kim J (2005) Systematic phase control of periodic mesoporous organosilicas using Gemini surfactants. J Mater Chem 15(44):4711–4717

[40] Czechura K, Sayari A (2006) Synthesis of MCM-48 silica using a Gemini surfactant with a rigid spacer. Chem Mater 18(17):4147–4150

[41] Danino D, Talmon Y, Zana R (1995) Alkanediyl-α, ω-bis(dimethylalkylammonium bromide) surfactants (dimeric surfactants). 5. Aggregation and microstructure in aqueous solutions. Langmuir 11(5):1448–1456